# Homonuclear and Heteronuclear NMR Studies of a Statherin Fragment Bound to Hydroxyapatite Crystals

**Vinodhkumar Raghunathan,[†,‡] James M. Gibson,[‡,||] Gil Goobes,[†] Jennifer M. Popham,[†] Elizabeth A. Louie,[†,§] Patrick S. Stayton,[‡] and Gary P. Drobny*[,†]**

*Departments of Chemistry and Bioengineering, University of Washington, Box 351700, Seattle, Washington 98195*

*Received: November 16, 2005; In Final Form: January 31, 2006*

Acidic proteins found in mineralized tissues act as nature's crystal engineers, where they play a key role in promoting or inhibiting the growth of minerals such as hydroxyapatite (HAP), $Ca_{10}(PO_4)_6(OH)_2$, the main mineral component of bone and teeth. Key to understanding the structural basis of protein−crystal recognition and protein control of hard tissue growth is the nature of interactions between the protein side chains and the crystal surface. In an earlier work we have measured the proximity of the lysine (K6) side chain in an SN-15 peptide fragment of the salivary protein statherin adsorbed to the Phosphorus-rich surface of HAP using solid-state NMR recoupling experiments. $^{15}N\{^{31}P\}$ rotational echo double resonance (REDOR) NMR data on the side-chain nitrogen in K6 gave rise to three different models of protein−surface interaction to explain the experimental data acquired. In this work we extend the analysis of the REDOR data by examining the contribution of interactions between surface phosphorus atoms to the observed $^{15}N$ REDOR decay. We performed $^{31}P-^{31}P$ recoupling experiments in HAP and $(NH_4)_2HPO_4$ (DHP) to explore the nature of dipolar coupled $^{31}P$ spin networks. These studies indicate that extensive networks of dipolar coupled $^{31}P$ spins can be represented as stronger effective dipolar couplings, the existence of which must be included in the analysis of REDOR data. We carried out $^{15}N\{^{31}P\}$ REDOR in the case of DHP to determine how the size of the dephasing spin network influences the interpretation of the REDOR data. Although use of an extended $^{31}P$ coupled spin network simulates the REDOR data well, a simplified $^{31}P$ dephasing system composed of two spins with a larger dipolar coupling also simulates the REDOR data and only perturbs the heteronuclear couplings very slightly. The $^{31}P-^{31}P$ dipolar couplings between phosphorus nuclei in HAP can be replaced by an effective dipolar interaction of 600 Hz between two $^{31}P$ spins. We incorporated this coupling and applied the above approach to reanalyze the $^{15}N\{^{31}P\}$ REDOR of the lysine side chain approaching the HAP surface and have refined the binding models proposed earlier. We obtain $^{15}N-^{31}P$ distances between 3.3 and 5 Å from these models that are indicative of the possibility of a lysine−phosphate hydrogen bond.

## Introduction

One of many important functions that proteins undertake in the regulation of biomineralization is the direct control of nucleation and growth of biomineral crystals.[1−3] Despite the important roles that they play and the significance that the structure/function relationships of these proteins have in the fields of medicine and dentistry, remarkably little is known about the underlying mechanisms whereby proteins regulate hard tissue growth. A better understanding of the biomolecular recognition mechanisms involved in biomineralization could provide important design principles for the development of calcification promoters and inhibitors in cardiology, urology, dentistry, and orthopedics.

Calcium hydroxyapatite ($Ca_{10}(PO_4)_6(OH)_2$, HAP), an important constituent of all major mammalian mineralized tissues, including enamel, dentine cementum, and bone,[4] has widespread use in chromatography columns, in catalysis supports, and as a bioactive load-bearing implant.[5−11] Salivary statherin is a 43-amino-acid acidic phosphopeptide found in the saliva, which functions biologically to inhibit the nucleation and growth of calcium phosphate minerals and also acts as a boundary lubricant.[12−17] Statherin and SN-15, the N-terminal 15-residue fragment of statherin, are known to bind strongly to HAP crystals, with the first five amino acids in the N-terminus of statherin, comprising one aspartic acid, two phosphorylated serines, and two glutamic acid residues, being important in the adsorption to HAP.[14]

A number of solid-state NMR (ssNMR) studies of the secondary structure and dynamics of statherin and SN-15 on HAP crystal surfaces have been reported.[18−21] The most recent study that we performed on the interface of SN-15 and HAP involved measuring distances from isotopic spin labels[22] on peptide side chains to NMR-active nuclei in the HAP surface using rotational echo double resonance (REDOR).[23a,b] In this study, it was found that the $^{15}N\epsilon$ spin of the unique lysine side chain in statherin interacts with two or more $^{31}P$ spins in the HAP surface. However, if an observed spin is dipolar coupled to two or more dephasing spins and the heteronuclear dipolar

* Author to whom correspondence should be addressed. E-mail: drobny@chem.washington.edu

[†] Department of Chemistry.

[‡] Department of Bioengineering.

[§] Present address: Institute of Imaging Science, Department of Radiology and Radiological Sciences, Vanderbilt University, 1161 21st Ave. South, R-1302 MCN Nashville, TN 37232.

[||] Present address: Department of Chemistry and Chemical Biology, Rensselear Polytechnic Institute, Troy, NY 12180.

10.1021/jp056644g CCC: $33.50 
Published on Web 04/18/2006

couplings are unequal, then the REDOR response is modulated by the homonuclear dipolar couplings between the spins of the dephasing channel.[24,25] In the case of the lysine side chain of statherin in proximity to the HAP surface, the homonuclear couplings between $^{31}$P spins in the HAP surface modulate the $^{15}$N{$^{31}$P} REDOR response, which would normally be due to the $^{15}$N−$^{31}$P dipolar couplings alone. One of the models used in the study incorporated a single $^{31}$P−$^{31}$P homonuclear coupling of 1800 Hz, corresponding to a $^{31}$P−$^{31}$P distance of 2.2 Å, to simulate the REDOR dephasing curve. This $^{31}$P−$^{31}$P distance is smaller than expected for the environment of the HAP lattice and was proposed to be likely the result of simplifying the structure of the HAP lattice that lies near the lysine side chain, probably by reducing the number of coupled $^{31}$P spins that ultimately affect the REDOR dephasing.

In a REDOR experiment involving two or more inequivalent heteronuclear couplings between a protein and a surface, it is important to understand the local environments of the dephasing spins on the surface. The present work aims in part to extend the analysis in ref 22 by characterizing the $^{31}$P dipolar coupling network in HAP using homonuclear recoupling techniques. This information is incorporated into the REDOR simulations to accurately account for the effect of the homonuclear couplings.

Several ssNMR studies have been carried out on HAP and other calcium phosphates. These studies primarily identified specific calcium phosphate phases to obtain fingerprints.[26] For example, Pang[27] used the REDOR pulse sequence to understand the incorporation of fluoride ions into the HAP lattice during an exchange reaction. $^{1}$H NMR multiple quantum studies have been carried out on fluorohydroxyapatite samples to understand fluoride incorporation and lack of local stoichiometry in different kinds of hydroxyapatite samples.[26]

Although the ssNMR studies mentioned above used multiple quantum techniques to define HAP stoichiometry, none utilized $^{31}$P NMR to understand crystallinity and stoichiometry in HAP. $^{31}$P NMR is a powerful technique that has been extensively used to understand structure, connectivities, vacancy ordering, and host−guest interactions in phosphate glasses, crystalline phosphates, phosphide semiconductor alloys, and inorganic thiophosphates.[28−31] Günne et al. have applied $^{31}$P double quantum filtered two-dimensional (2D) NMR in conjunction with crystal structure studies to understand local environments of sites in $LiP_5$.[32] Bertmer and Eckert have obtained mean heteronuclear couplings from multispin systems by applying second moment analysis to the initial part of REDOR dephasing curves.[33] Homonuclear couplings between dephasing spins were not included in their analysis. In our case, the effect of the homonuclear couplings between the dephasing spins is observed in the later time points of the REDOR dephasing curve.

Recently Günne has developed pulse sequences based on the symmetric C/R pulse sequences for distance measurements in dense dipolar phosphate networks.[34] Most of the aforementioned studies have investigated systems in which two atoms are connected through a bridging oxygen atom. To the best of our knowledge there have been two $^{31}$P double quantum NMR studies on orthophosphates, i.e., phosphates without through-bond connectivity. The first study utilized a BABA (back to back sequence)-based double quantum 2D NMR experiment on cadmium phosphate to measure the spatial proximity of crystallographically inequivalent tetrahedra.[35] In the second study, Tseng et al. applied $^{31}$P double quantum NMR based on the finite pulse radio-frequency-driven dipolar recoupling (fpRFDR)[36,37] sequence to HAP and octacalcium phosphate at high spinning speeds.[38] This study has been carried out as a feasibility study to explore the efficiency of creating $^{31}$P double quantum polarization. Quantitative information regarding distances between the phosphate tetrahedra was not obtained from either of these studies.

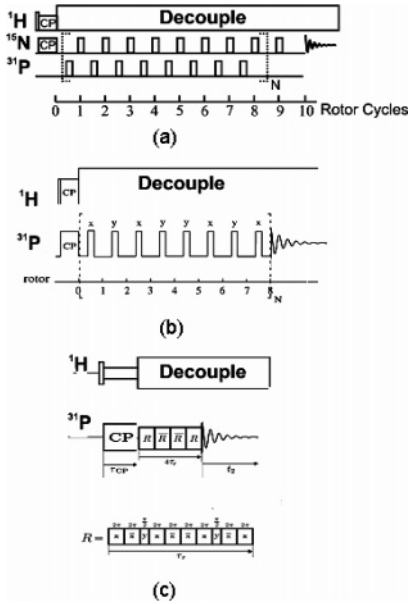


**Figure 1.** Pulse sequences: (a) REDOR, (b) SEDRA, (c) DRAWS.

An important experimental component of the present study is measurements of homonuclear dipolar couplings through recoupling experiments. In this article, $^{31}$P homonuclear recoupling experiments based on simple excitation for dephasing rotational amplitudes (SEDRA)[39] and dipolar recoupling with a windowless sequence (DRAWS)[40] were used to explore the manifestation of homonuclear couplings originating from within the phosphate network of HAP and diammonium hydrogen phosphate (DHP). On the basis of the information obtained from these experiments, the effect of the homonuclear couplings on the REDOR distance measurements was also investigated. We extend our previously mentioned preliminary work[22] on surface-to-side-chain REDOR experiments of the unique lysine K6 side chain of the SN-15 (DpSpSEE$^{15N}$KFLRRIGRFG) peptide bound to HAP by reanalyzing the results to incorporate the findings of this manuscript and show that the contribution from homonuclear couplings between $^{31}$P in the phosphate network can be approximated by a pair coupling of no larger than 600 Hz. Therefore the model that attributes the observed REDOR decay to an 1800 Hz coupling is not realistic even when taking into account the full $^{31}$P network. Inclusion of the contribution from the $^{31}$P network in the form of a $^{31}$P spin pair with a larger effective homonuclear dipolar interaction is shown to give rise to a bimodal distribution model in the simplest case where 44% of the peptide molecules are adsorbed with a N−P distances of 3.3 and 3.5 Å and the rest with N−P distances of 4.8 and 5.1 Å.

## Experimental Section

**NMR Pulse Sequences.** *REDOR.* REDOR is a well-established technique for measuring the distance between two nuclei in an isolated heteronuclear spin pair.[23] The version of REDOR used in this work is shown in Figure 1a. The reference experiment $S_0$ is carried out to compensate for the loss of echo amplitude due to $T_2$ relaxation and has pulses only in the observe channel. In the S experiment, each rotor period has two pulses applied to both the observe and dephasing channels. The primary

cycle time for this pulse sequence is two rotor periods. At the end of two rotor periods, signal dephasing due to CSA interactions is refocused. The signal dephasing due to heteronuclear dipolar coupling is not refocused.

In the case of isolated spin pairs, the REDOR dephasing can be fit to a universal REDOR curve,[23b] but this is not the circumstance when strongly coupled spins exist in the dephasing channel. In this case the pulse sequence applied in the S experiment on the dephasing channel is equivalent to a SEDRA/RFDR experiment that recouples homonuclear spins. In the case that dispersion exists in the heteronuclear dipolar interactions, the homonuclear dipolar interactions will modulate the REDOR response obtained from the pulse sequence in Figure 1a.

*SEDRA.* Figure 1b depicts the pulse sequence employed to perform the SEDRA experiment.[39] This pulse sequence relies on synchronously applied rf pulses with a basic time unit of two rotor periods. A single $\pi$ pulse is applied every rotor period. The SEDRA pulse sequence refocuses dephasing of the signal caused by the chemical shift anisotropy (CSA) interaction while allowing dephasing caused by the dipolar interaction between coupled spins. The experiment is then repeated as increments of SEDRA cycles to obtain the SEDRA dephasing curve, which is then fitted by simulations to obtain internuclear distances.

*DRAWS.* Figure 1c shows a representation of the DRAWS pulse sequence, which has been shown to be less sensitive to large CSA nuclei than other DQ filtered sequences.[40] The pulse sequence usually starts by creating transverse magnetization. A DRAWS supercycle consists of two R and two $\bar{R}$ blocks supercycled as R$\bar{R}\bar{R}$R to suppress the effects due to the CSA interactions.[41,42] Each R element is composed of 10 radio frequency (rf) pulses with phases and flip angles as shown in Figure 1c and occupies exactly one rotor period. The supercycle is generally repeated *n* times to obtain a dephasing curve, similar to that of the SEDRA curve that can be simulated to obtain the homonuclear dipolar couplings.

**Materials.** HAP was obtained from Allison Campbell's laboratory at the Battelle Pacific Northwest National Laboratories. The preparation and the characterization of this HAP have been described elsewhere.[12] DHP was obtained from Sigma-Aldrich and used without any further modification. Preparation of the isotopically enriched SN-15 and binding of the peptide to HAP samples followed procedures that have been described elsewhere.[22]

**Transmission Electron Microscopy.** The transmission electron microscopy (TEM) image of the hydroxyapatite crystals was obtained on a Philips EM 420 T transmission electron microscope at an accelerating voltage of 120 kV and a with a $LaB_6$ filament.

**NMR Experiments.** Samples of SN-15 bound to HAP were processed and packed into the rotor as described earlier.[12] DHP was crushed into a fine powder and packed into the NMR rotor. HAP was washed several times with doubly distilled water and dried under atmosphere before packing into an NMR rotor. Solid-state NMR experiments were carried out on a 4.68 T home-built spectrometer operating at a $^{31}$P Larmor frequency of 80.9984 MHz and a $^{1}$H frequency of 200.092 MHz with a 5 mm home-built triply resonant magic angle spinning probe[43] at room temperature. Spinning rates were maintained by a home-built spin-rate controller. Experimental errors in the homonuclear recoupling experiments were estimated through three repetitions of the experiment. In case of the REDOR, experimental errors were estimated from the signal-to-noise ratios.

*DHP*. The $^{1}$H$-^{31}$P cross polarization magic angle spinning (CPMAS) on DHP used a $^{1}$H $\pi/2$ pulse width of 5.8 $\mu$s and a 2 ms CP contact time. The DRAWS experiment on this sample was performed at a spinning speed of 2557 $\pm$ 4 Hz to ensure that the $^{1}$H decoupling power had a 3:1 ratio to the $^{31}$P rf power used in the experiment.[44] The continuous wave decoupling power used on the experiments of DHP was 73 kHz. The SEDRA experiment was performed at the same spinning speed and used a $\pi$ pulse duration of 22 $\mu$s. For the SEDRA experiment the data was acquired every eight rotor cycles.

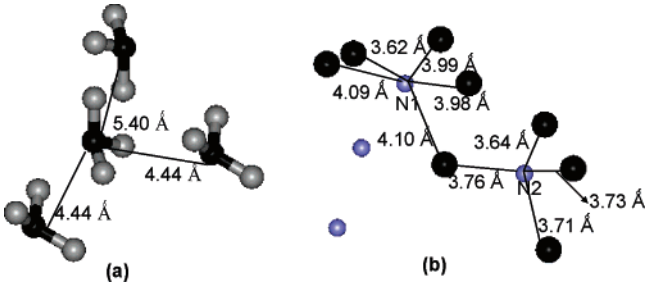


**Figure 2.** (A) Crystal structure of diammonium hydrogen phosphate showing the nearest neighbors of any chosen phosphate group. (B) The $^{31}$P dipolar field around the $^{15}$N spins. Black balls denote the phosphorus atoms, gray balls denote the oxygen atoms, and the blue balls denote the $^{15}$N atoms.

*HAP*. The $^{1}$H$-^{31}$P CPMAS on HAP used a $^{1}$H $\pi/2$ pulse width of 5.45 $\mu$s and a 2 ms contact time. All the experiments on HAP and related samples were performed at a spinning speed of 5000 $\pm$ 4 Hz. The number of transients acquired was either 128 or 256. The pulse widths used during the DRAWS cycles were calibrated to be rotor synchronous. The SEDRA experiments used a $^{31}$P $\pi$ pulse duration of 11.76 $\mu$s.

**Spin Dynamics Simulations.** Numerical simulations of the experimental data were performed using the NMR simulation programs SIMPSON[45] and SPINEVOLUTION[46] employing the direct algorithm without any relaxation. Larger crystallite tests were explored to test convergence of simulations. Convergence of results from the two programs was verified for simulations of up to five-spin systems. For larger spin clusters (up to nine spins) the SPINEVOLUTION program was used. Powder averages were obtained using a minimal set of 54 $\{\alpha,\beta\}$ Euler angles specified by the Zaremba$-$Conroy$-$Wolfsberg[47,48] scheme and 5 $\gamma$ angles. In all of the simulations, the magnetization of a chosen central spin was propagated in the dipolar field of all its nearest neighbors.

The CSAs of the $^{31}$P nuclei in the crystals were calculated by Herzfeld$-$Berger sideband intensity analysis[49] of the CPMAS spectrum using the HBA program[50] whenever possible and confirmed against known values.[51] The CSA orientations with respect to the molecular frame were obtained from literature.[52$-$54] The CSA of the $^{15}$N nucleus in the molecule was found to be small and was therefore neglected. All dipolar interaction parameters were computed from distances and orientations of P$-$P and P$-$N vectors in the crystal and referenced to the CSA PAS frame of the observed P atom in calculations.

**Crystal Structures.** *DHP*. DHP is known to crystallize in the space group $P21/c$ with unit cell of dimensions $a = 11.04$ Å, $b = 6.70$ Å, and $c = 8.03$ Å. Each unit cell contains four molecules that are symmetry-related and closely packed.[55] The crystal structure of $(NH_4)_2HPO_4$ depicting the surroundings of an atom is shown in Figure 2a. All of the phosphate moieties are crystallographically equivalent. Each atom is surrounded by three nearest neighbor phosphate $^{31}$P spins lying within a radius of 6 Å. Two of these atoms are equidistant at 4.44 Å corresponding to a dipolar coupling of 226 Hz. The third neighbor is at a distance of 5.40 Å. The two nitrogen atoms in

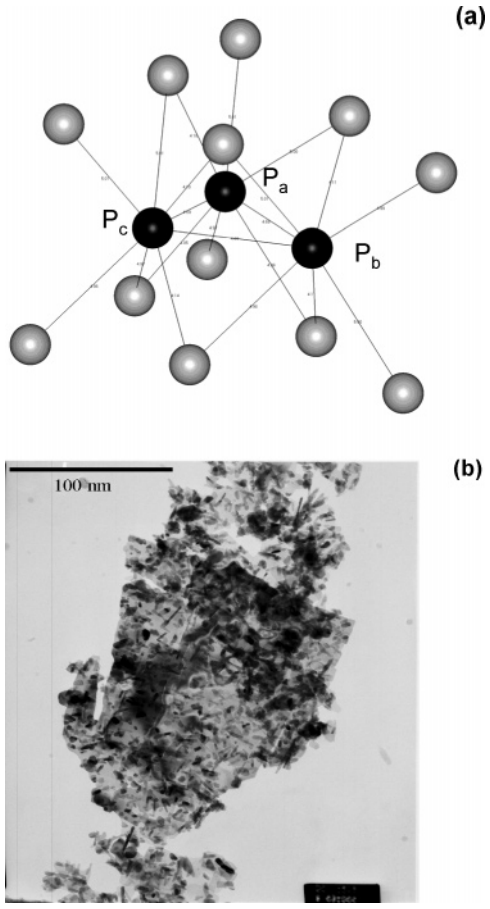


**Figure 3.** (a) Crystal Structure of HAP showing only the P atoms. The dark balls denote the three different kinds of central atoms $P_a$, $P_b$, and $P_c$, which are labeled, and the gray balls depict all the nearest neighbors under a distance of 5.1 Å (b) TEM image indicating the heterogeneous morphology of the HAP crystals used in the study.

the ammonium groups, annotated by N1 and N2 in Figure 2b, are crystallographically inequivalent and are slightly chemically shifted from each other. The phosphate groups are identical and appear as a single line in the $^{31}$P CPMAS spectrum.

*HAP*. The arrangement of $^{31}$P spins and the local dipolar connectivities between $^{31}$P spins observed in the crystal structure of HAP are complex. Stoichiometric synthetic HAP crystallizes in the monoclinic space group $P2_1/b$ with cell constants $a$ = 9.4214 Å, $b$ = 18.8428 Å, and $c$ = 6.8814 Å.[56] This structure is closely related to the hexagonal HAP crystal structure except for the loss of inversion symmetry. The hexagonal phase can be obtained through an order−disorder transition at a higher temperature from the monoclinic phase.[57] There are three crystallographically different kinds of $^{31}$P sites $P_a$, $P_b$, and $P_c$. The local dipolar environment of these three different sites with respect to nearby $^{31}$P atoms is slightly different. Unlike in the case of diammonium hydrogen phosphate in HAP the three crystallographically distinct $^{31}$P spins have at least nine nearest neighbor $^{31}$P spins within a distance of 5.5 Å as shown in Figure 3a. The exact distances of the nearest neighbors are tabulated in Table 2. Only one line is seen in the NMR spectrum indicating that the chemical shifts of these sites are the same.[26] The CSA magnitudes used in the simulations were obtained from ref 51. The morphology of the crystals was studied using transmission electron microscopy. The micrograph shows the presence of a heterogeneous distribution of several crystallites of different sizes and shapes ranging from 50 to 400 nm (Figure 3b).

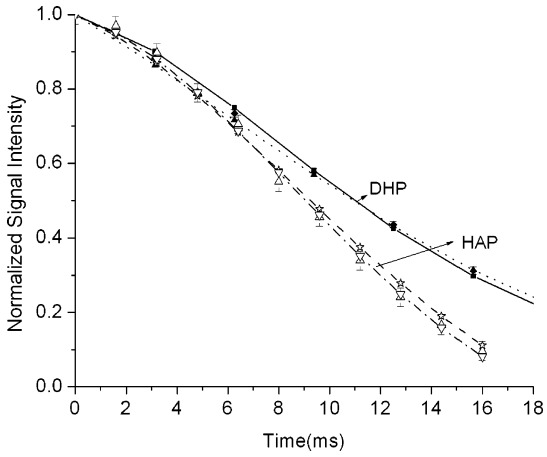


**Figure 4.** SEDRA dephasing experiments on (i) DHP. The dark diamonds are the experimental data; dark squares are the three-spin simulation of the crystallographic arrangement with two nearest neighbors, and the dark triangles denote the simulation assuming just a two-spin system with a P−P distance of 3.59 Å. SEDRA dephasing experiments on (ii) HAP. Open triangles are the experimental data. The open stars represent the nine-spin simulation of the crystallographic arrangement of a central atom with its nearest neighbors, and the inverted open triangles denote the two-spin equivalent simulation corresponding to a P−P distance of 3.1 Å.

**TABLE 1: Interatomic Distances in $(NH_4)_2HPO_4$[a]**

| P−N1 distance | P−N2 distance | P−P distance |
|---|---|---|
| 3.62 Å | 3.64 Å | 4.44 Å |
| 3.98 Å | 3.71 Å | 4.44 Å |
| 3.99 Å | 3.76 Å | 5.40 Å |
| 4.09 Å | 3.78 Å | |
| 4.10 Å | | |

[a] P−N distances are from N1/N2 to $^{31}$P nearest neighbors. $^{31}$P−$^{31}$P couplings are to nearest neighbors lying within a sphere of radius 6 Å. See Figure 2.

**TABLE 2: $^{31}$P−$^{31}$P nearest Neighbor Distances Lying within a Sphere of Radius 6 Å in Monoclinic HAP for the Three Different Crystallographic Sites**

| $P_a$ | $P_b$ | $P_c$ |
|---|---|---|
| 4.05 Å | 4.10 Å | 4.10 Å |
| 4.18 Å | 4.10 Å | 4.14 Å |
| 4.69 Å | 4.69 Å | 4.69 Å |
| 4.69 Å | 4.69 Å | 4.69 Å |
| 4.97 Å | 4.98 Å | 4.97 Å |
| 4.99 Å | 4.99 Å | 4.98 Å |
| 5.00 Å | 5.00 Å | 5.00 Å |
| 5.01 Å | 5.01 Å | 5.01 Å |

## Results

**SEDRA Results.** *DHP*. The normalized $^{31}$P SEDRA signal decay shown in Figure 4 (dark diamonds) indicates the presence of $^{31}$P−$^{31}$P dipolar couplings. Simulations of $^{31}$P signal dephasing shown in Figure 4 (dark squares) using the two largest P−P couplings of 225 Hz corresponding to the first two nearest neighbors at 4.44 Å from the crystal structure gave excellent fits to the data set. A transverse relaxation rate of 20 Hz was incorporated in these calculations to account for additional slower decay of the magnetization.[58] If the SEDRA data are analyzed assuming a two-spin system, then the data can also be simulated well with a much stronger dipolar coupling of 425 Hz, corresponding to a $^{31}$P−$^{31}$P distance of 3.59 Å (dark triangles) and transverse relaxation of 40 Hz. This distance is unrealistic based on the crystal structure data, but it describes the cumulative effect of the two homonuclear couplings in the total dephasing observed.

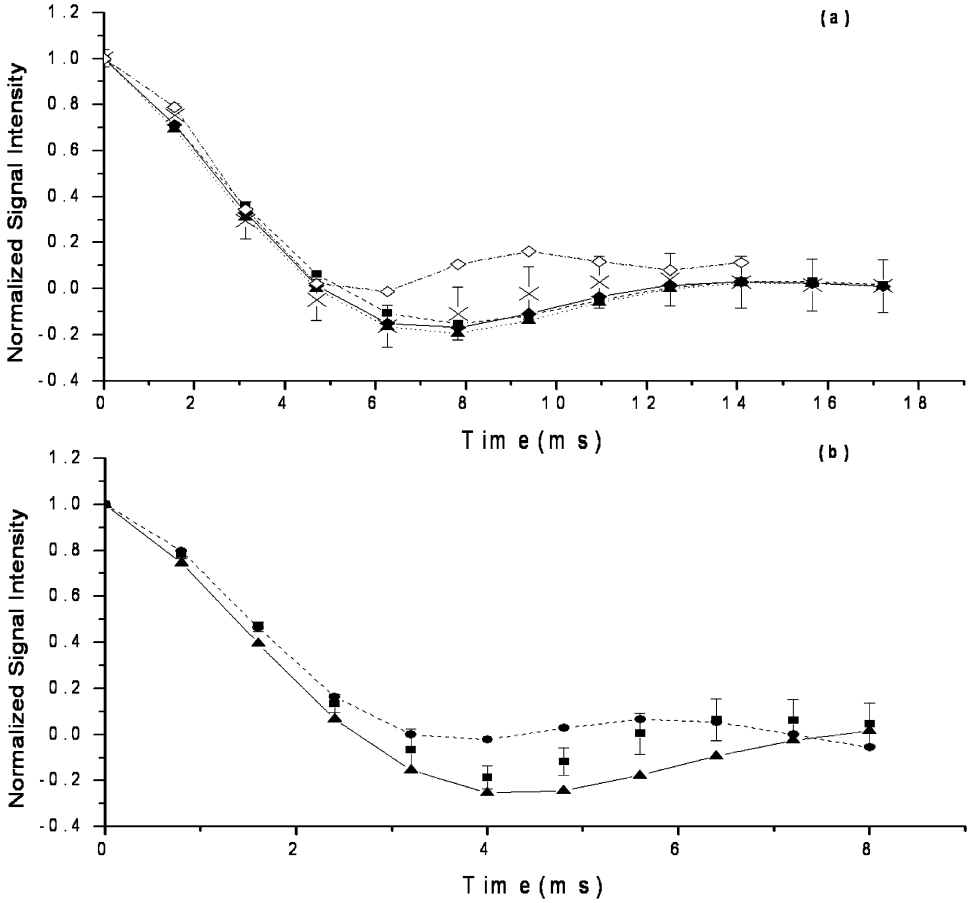


**Figure 5.** (a) DRAWS dephasing experiment on $(NH_4)_2HPO_4$ as represented by the crosses. The filled triangles, filled squares, and filled diamonds represent three-, four-, and six-spin simulations where the number of neighbors is progressively increased in the simulation. The fit improves with an increasing number of spins in the spin system. Open diamonds denote the effective two-spin simulation with a dipolar coupling of 425 Hz. (b) DRAWS dephasing experiment on $Ca_{10}(PO_4)_6(OH)_2$ (HAP). Experimental data are denoted by the filled squares. The nine-spin simulation of the crystallographic arrangement of a central atom with its nearest neighbors is denoted by the filled triangles. The effective two-spin simulation with a dipolar coupling 600 Hz coupling is denoted by the filled circles.

*HAP*. The dipolar field around the $^{31}P$ spins in HAP is much more complex than the above case. The data (Figure 4, open triangles) can be simulated well by a nine-spin simulation (Figure 4, open stars), which includes eight out of the nine nearest neighbors around the central spin. A more accurate simulation would be a 15-spin simulation, which would include the three central spins depicted in Figure 3a in the presence of all their nearest neighbors. In this case a transverse relaxation rate of 30 Hz was included in the simulation. Additionally, the experiment was performed at two different rf power values (data not shown). The same spin arrangement and transverse relaxation rates yielded excellent fits in both cases. The effective two-spin homonuclear coupling that fits the data is 600 Hz corresponding to a $^{31}P-^{31}P$ distance of 3.1 Å (Figure 4, inverted open triangles). A transverse relaxation of 17 Hz was included in the simulation.

**DRAWS Dephasing Results.** *DHP*. DRAWS dephasing data for $(NH_4)_2HPO_4$ are shown in Figure 5a (crosses). As in the SEDRA experiment, a DRAWS dephasing experiment signal decays due to the homonuclear dipolar interaction between the spins. But the DRAWS experiment is much more sensitive to smaller dipolar couplings and farther neighbors than the SEDRA experiment. This can be observed from Figure 5a. The initial part of the decay curve is reproduced by including only the nearest neighbors as seen from the three-spin simulation (Figure 5a, filled triangles with the dotted line). The fit improves slightly with the inclusion of more spins in the simulation as can be seen from the four (Figure 5a, filled squares with the dotted lines) and the six (Figure 5a, filled diamonds with the solid line) spin simulations. An exponential decay of 110 Hz has been included in these simulations to account for transverse relaxation. The decay part of the DRAWS dephasing can also be fit with a two-spin approximation of 425 Hz just as in the case of SEDRA (Figure 5a, open diamonds), but it fails to fit the oscillatory regime. The oscillatory regime in the DRAWS dephasing is probably more sensitive to long-range couplings than the SEDRA experiment.

*HAP*. The result of the DRAWS dephasing experiment is shown in Figure 5b (filled squares). These simulations are an average of three nine-spin simulations that considered only the nearest neighbors of each central spin (Figure 5b, filled triangles). A more accurate simulation would be a 15-spin simulation that would include the three central spins depicted in Figure 4a and all their nearest neighbors. There is a small divergence in the fit in the oscillatory regime, which would possibly improve with the addition of more spins to the spin system used in the simulation. A two-spin approximation (Figure 5b, filled circles) with a 600 Hz coupling fits the decay well, but it fails to reproduce the oscillatory regime of the dephasing curve just as in the case of DHP.

**$\{^{15}N\}^{31}P$ REDOR on DHP.** A recent $^{15}N\{^{31}P\}$ REDOR study of DHP concluded that accurate knowledge of the geometry of the dephasing spin system is required for a faithful simulation of the REDOR data and truncation of the dephasing spin system results in the underestimation of distances between dephasing spins.[25] In light of this, the impact of dephasing spin

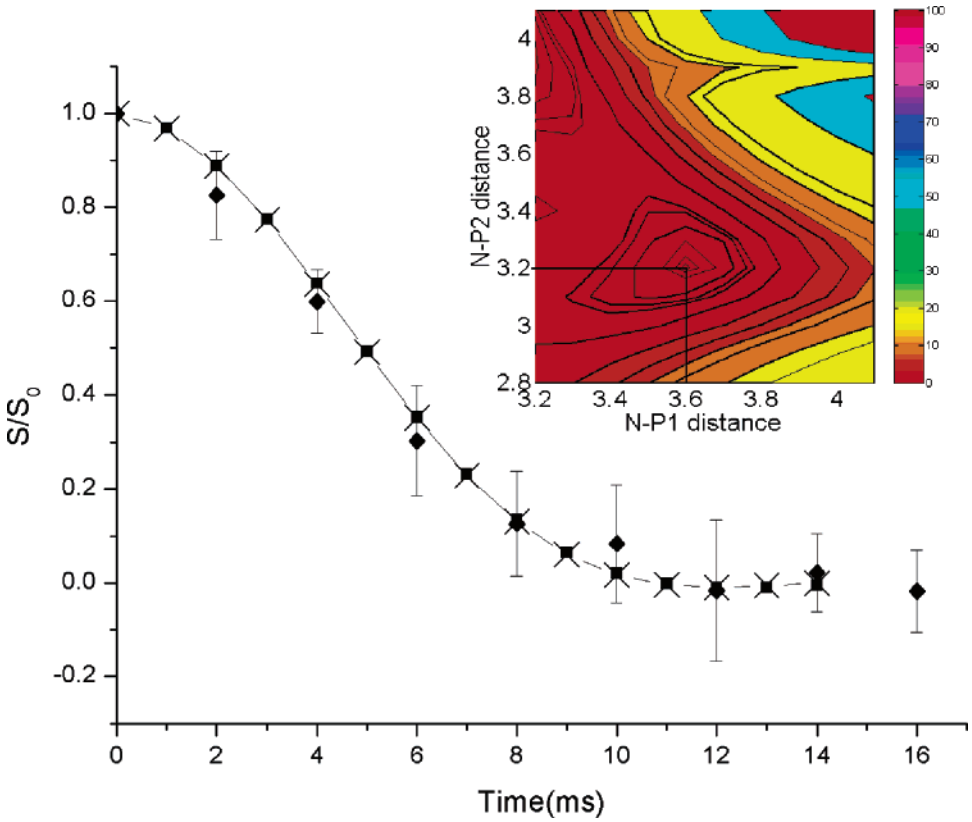


**Figure 6.** Statistical $\chi^2$ analysis of the effective three-spin simulation of the $^{15}N\{^{31}P\}$ REDOR in $(NH_4)_2HPO_4$ indicates a minimum at distances of 3.64 and 3.22 Å. These values are close to 0.5 Å within the $^{15}N-^{31}P$ distances in $(NH_4)_2HPO_4$. The filled diamonds are the experimental data while the filled squares denote the six-spin simulation of the $^{15}N\{^{31}P\}$ REDOR with a $^{15}N$ spin surrounded by five $^{31}P$ neighbors as shown in Table 1. The crosses denote the simulation with the distances showing the minimum in the $\chi^2$ analysis.

system truncation is further explored by a $\chi^2$ analysis of the $^{15}N\{^{31}P\}$ REDOR data for the N1 spin in DHP. Assuming a three-spin NPP system with the $^{31}P-^{31}P$ coupling set to the effective dipolar coupling of 425 Hz obtained from the SEDRA and DRAWS experiments, a $\chi^2$ statistical analysis,[59] shown in Figure 6 was performed by varying both the $^{15}N-^{31}P$ distances. This shows a minimum occurring at distances of 3.6 and 3.2 Å. The fitting of this particular simulation (Figure 6, crosses) to the experimental REDOR curve (Figure 6, filled diamonds) is as good as the simulation that incorporates all five $^{15}N-^{31}P$ distances ranging from 3.62 to 4.10 Å as shown in Table 1 (filled squares) seen from Figure 6. The four other heteronuclear dipolar couplings manifest as a stronger dipolar coupling and thus a shorter distance, which is within 0.5 Å of the shortest distance present in the crystal. The statistically determined distances from a simplified lower-dimension model are close to the actual ones present in the crystal within 0.5 Å.

**$\{^{15}N\}^{31}P$ REDOR on SN-15 bound to HAP.** A preliminary $\{^{15}N\}^{31}P$ REDOR study of the K6 side chain of the SN-15 peptide bound to the HAP surface was published earlier[22] and is shown in Figure 7a. In ref 22, simulation of the REDOR data was hindered by lack of knowledge about the size of the dephasing spin system, and therefore three simplified models of side chain−surface interactions were considered. In Figure 7a, the solid line represents a system where the K6 $^{15}N$ is 3.7 Å from one $^{31}P$ spin and 4.4 Å from a second with the two $^{31}P$ spins being 2.2 Å apart. The long dashed line represents the system where a bimodal distribution was assumed—40% of the $^{15}N$ K6 spin remain uncoupled, and 60% are 3.1 Å from a $^{31}P$ spin. The short dashed line represents an NPP system that is nearly linear in its geometry with $^{15}N-^{31}P$ distances of 3.7 and 4.0 Å and a P−N−P angle of 170°.

## Discussion

The fundamental aim in the engineering of biomineralization is to gain knowledge about the factors that cause a regulation protein to recognize an inorganic mineral surface. The determination of protein contact points with the surface involves using the REDOR experiment. REDOR has been used successfully in the past for isolated two-spin systems. In the present case, REDOR is complicated by the fact that the surface consists of a bath of coupled dephasing spins with homonuclear couplings that affect the REDOR dephasing. In the Results section the dipolar coupling networks for DHP and HAP were studied using homonuclear dipolar recoupling techniques. In particular, $^{31}P$ dipolar coupling networks in DHP were studied using homonuclear recoupling techniques, and the resulting information was used to fit $^{15}N\{^{31}P\}$ REDOR data by a $\chi^2$ analysis. We will proceed along the same basic lines in the analysis of the $^{15}N\{^{31}P\}$ REDOR data for the $^{15}N$ spin in the side chain of K6 with the $^{31}P$ spins in the HAP surface.

The first model described in the preliminary study of SN-15 on HAP involves a three-spin NPP system with a $^{31}P-^{31}P$ distance of 2.2 Å corresponding to a homonuclear coupling of 1800 Hz.[22] It was proposed that, given the constraints of HAP geometry, such a short P−P distance is unrealistic and probably due to a result of truncating an extended $^{31}P-^{31}P$ coupling network. However the conclusion borne out by the results of the homonuclear dipolar recoupling experiments described in this manuscript find that the highly extended P−P coupling network in HAP manifests itself as a homonuclear dipolar coupling of 600 Hz. Therefore we have reanalyzed the REDOR results of the earlier manuscript. A $\chi^2$ analysis of the data in ref 22, shown in Figure 7b, assumes an NPP system with a

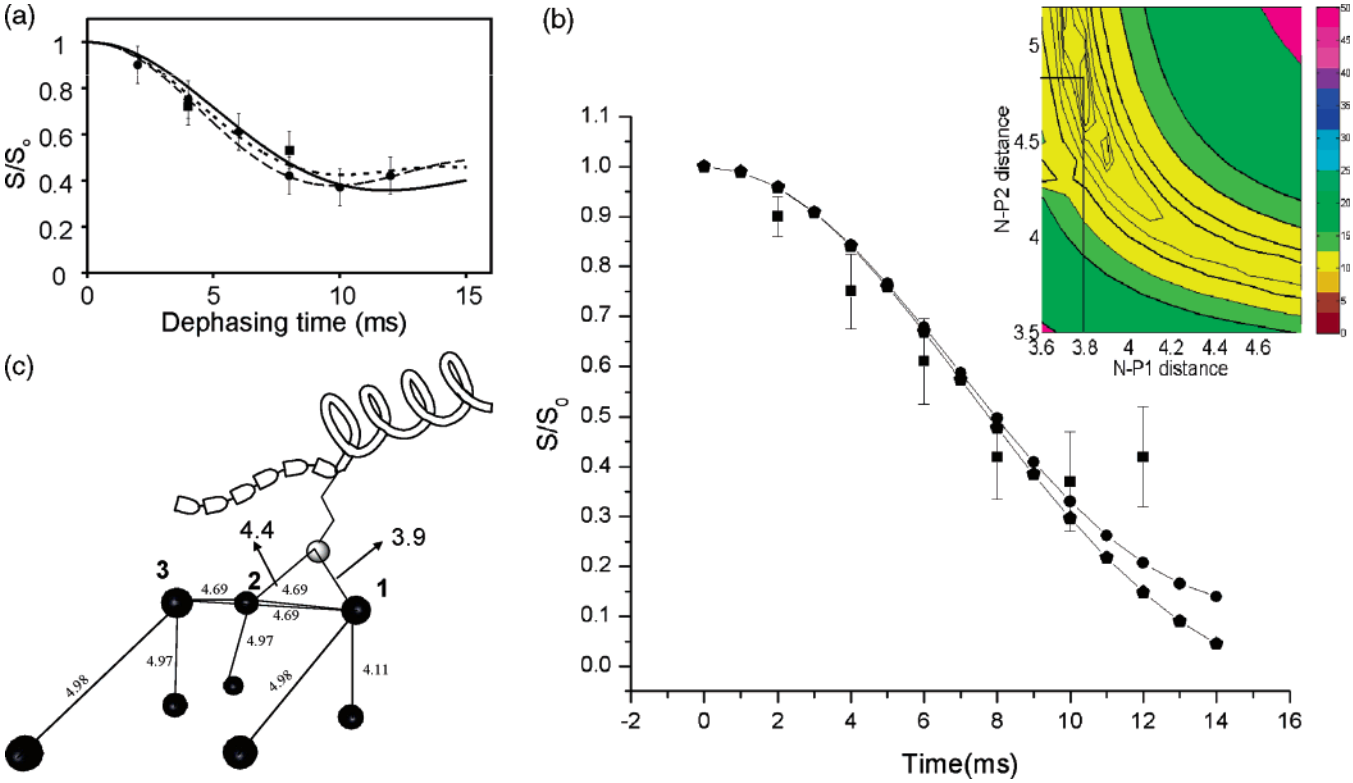


**Figure 7.** (a) $^{15}N\{^{31}P\}$ REDOR was performed on an SN-15 sample bound to HAP. The filled circles are experimental data from the lyophilized SN-15 bound to HAP, while the filled squares are experimental data from the hydrated sample. Three possible models that fit our REDOR data are shown. The solid line represents a system where the K6 $^{15}N$ is 3.7 Å from one $^{31}P$ spin and 4.4 Å from a second with the two $^{31}P$ spins being 2.2 Å apart. The long dashed line represents the system where a bimodal distribution exists—40% of the $^{15}N$ K6 spin remain uncoupled, and 60% are 3.1 Å from a $^{31}P$ spin. The short dashed line represents a system that is nearly linear in its geometry with $^{15}N-^{31}P$ distances of 3.7 and 4.0 Å. (b) Statistical $\chi^2$ analysis of binding of $^{15}N$ K6 of SN-15 to HAP indicating well-defined minimum distances of 3.8 and 4.8 Å suggesting a possible hydrogen bond between the K6 side chain and the HAP atoms. The filled squares are the experimental data while the filled circles denote the simulation that gives rise to the $\chi^2$ minimum, and the pentagons indicate the multiple-spin simulation of $^{15}N$ K6 approaching the (004) crystal plane of hydroxyapatite. (Parameters used for the simulation are defined thoroughly in part c.) (c) Model of a $^{15}N$ K6 side chain of SN-15 approaching the (004) crystal plane of hydroxyapatite. The figure depicts all of the spins that were used in the above-mentioned simulation. The dark circles denote the spins while the lighter shaded circle depicts the $^{15}N$ spin on the lysine side chain. The blocks on the peptide depict the six N-terminal residues of SN-15 that are known to be in an extended conformation.

**TABLE 3: $^{31}P-^{31}P$ nearest Neighbor Distances Lying within a Sphere of Radius 6 Å for the 004 Crystal Plane in Monoclinic HAP[a]**

| P1 | P2 |
|---|---|
| 4.69 Å (P2) | 4.69 Å (P1) |
| 4.69 Å (P3) | 4.69 Å (P3) |
| 4.98 Å | 4.98 Å |
| 4.11 Å | 4.97 Å |
| P3 is connected to another spin at a distance of 4.97Å | |

[a] The two spins P1 and P2 were assumed to be connected to the approaching $^{15}N$ lysine side chain.

$^{31}P-^{31}P$ effective dipolar coupling of 600 Hz and shows a well-defined minimum for $^{15}N-^{31}P$ distances of 3.8 and 4.8 Å from the $^{31}P$ spins (Figure 7b, filled circles).

In addition, to the simplified three-spin model, we have simulated a $^{15}N$ spin from the lysine side chain approaching two spins on the (004) crystal plane of HAP as shown in Figure 7c. These spins are connected to six other spins at distances shown in Table 3. We obtained a fit similar to the one obtained from the simple model, described above, but with slightly different $^{15}N-^{31}P$ distances of 3.9 and 4.4 Å (Figure 7b, filled pentagons).

Comparison of both the above simulations and the $^{15}N\{^{31}P\}$ REDOR data shows that the greatest disagreement occurs at long mixing times where the experimental REDOR data level out at higher $S/S_0$ values than displayed by the simulations. The leveling of the REDOR data can be addressed by using a distribution of distances as shown in Figure 8. In this case the fitting was obtained by assuming 44% of the K6 $^{15}N$ spins are at distances of 3.5 and 3.3 Å from the two spins and the remaining K6 $^{15}N$ spins are separated by 4.8 and 5.1 Å from the spins. In the simulations used in the distribution model, the $^{31}P$ spins have an effective dipolar coupling of 600 Hz. This is just one representative distribution. Numerous such distributions are possible given the heterogeneity of the sample arising from the presence of crystallites of various sizes with different exposed crystal faces. It is possible that there is no specificity displayed by the peptide to a particular crystal face and the peptide binds to different crystal faces with different distances ranging from 3.3 to 5.0 Å.

## Conclusions

To aid in the interpretation of data obtained from $^{15}N\{^{31}P\}$ REDOR studies of biomineralization proteins adsorbed onto HAP crystals, $^{31}P$ homonuclear recoupling experiments based on SEDRA and DRAWS were performed to understand and obtain effective homonuclear couplings in crystalline phosphate networks including HAP and DHP. Diammonium hydrogen phosphate was used as a model system to determine the effective size of dipolar coupled $^{31}P$ networks and to determine how the size of the dephasing spin network influences the interpretation of the REDOR data. In DHP, although use of an extended $^{31}P$

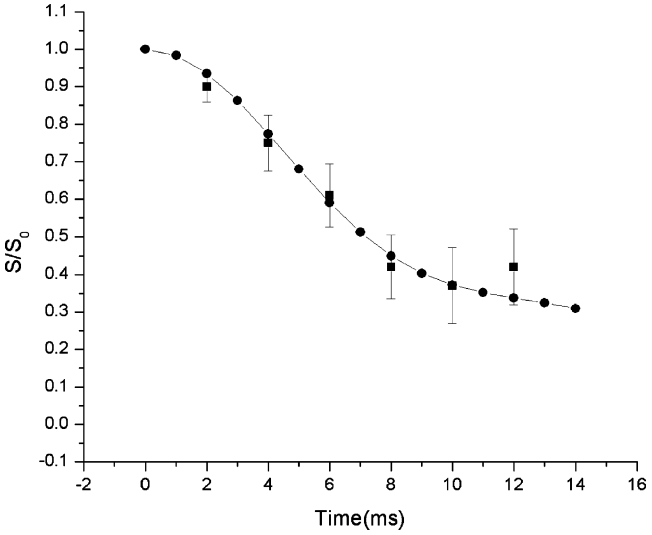


**Figure 8.** Representative distribution of distances between the $^{15}$N K6 side chain and spins on the HAP surface. The fitting simulation denoted by the filled circles is a linear combination of two NPP simulations with 44% of the K6 $^{15}$N spins at distances of 3.5 and 3.3 Å from the two spins, and the remaining K6 $^{15}$N spins are separated by 4.8 and 5.1 Å from the spins

coupled spin network simulates the REDOR data well, a simplified $^{31}$P dephasing system composed of two spins with a larger dipolar coupling also simulates the REDOR data and only perturbs the heteronuclear couplings slightly.

Because the $^{31}$P dipolar coupled network of HAP is large computational limitations preclude its use in simulations of $^{15}$N{$^{31}$P} REDOR experiments between the $^{15}$N in the unique lysine side chain of SN-15 and the $^{31}$P spins of the HAP surface. We have applied the same analysis as the DHP in the case of the lysine side chain approaching the HAP. This analysis yields $^{15}$N−$^{31}$P distances of 3.8 and 4.8 Å. The analysis of the REDOR data with a large number of dephasing spins yields $^{15}$N−$^{31}$P distances that are only slightly different. One of the successful fits results from the simulation models involving a distribution of distances from the $^{15}$N of the K6 side chain of SN-15 to the surface of HAP, with distances of 3.3, and 3.5 Å and 4.8 and 5.1 Å, respectively. In reality many such distributions can be discovered that might fit the data. All these distributions are possible given the heterogeneous nature of the HAP crystals and the possibility that the peptide might be binding to different crystal faces with slightly different distances. However in all the above models considered, the N−P distances obtained fall well within the realm of lysine−phosphate hydrogen bonds observed in complexes of proteins or peptides with nucleic acids and with inorganic phosphates.[60,61] On the basis of the results presented above, we hypothesize that the formation of a network of hydrogen bonds between protein side chains and components of the HAP surface could possibly constitute the underlying mechanism of the lysine side chain for specific protein−mineral recognition. Further studies of structure and dynamics on other side chains in SN-15 and full-length statherin will result in a better understanding of the interaction between the protein and the surface.

**Acknowledgment.** This work was supported by the National Science Foundation (EEC-9529161 and DMR-0110505) and the National Dental Institute (DE-12554). J.M.G. is supported by a training grant from the National Institute of Dental and Craniofacial Research (DE-07023). The authors thank Torgny Karlsson and Nathan Oyler for developing NMR processing software used in this work, Ora Schueler-Furman for providing the Rosetta models, Tom Murray for the acquisition of the TEM image, and Wendy Shaw for binding one sample. The data for the hydrated peptide was obtained at the Environmental Molecular Sciences Laboratory, a national scientific user facility sponsored by the Department of Energy's Office of Biological and Environmental Research and located at the Pacific Northwest National Laboratory.

## References and Notes

(1) Weiner, S.; Addadi, L. *J. Mater. Chem.* **1997**, *7*, 689−702.
(2) Coe, F. L.; Parks, J. H.; Asplin, J. R. *N. Engl. J. Med.* **1992**, *327*, 1141−1152.
(3) McCarty, D. J. *DM, Dis.−Mon.* **1994**, *40*, 258−299.
(4) Smith, D. A.; Connel, S. D.; Robinson, C.; Kirkham, J. *Anal. Chim. Acta* **2003**, *479*, 39−57.
(5) Zhang, X.; Gubbels, G. H. M.; Terpstra, R. A.; Metsellaar, R. *J. Mater. Sci.* **1997**, *32*, 235−243.
(6) Sun, L.; Berndt, C. C.; Gross, K. A.; Kucuk, A. *J. Biomed. Mater. Res.* **2001**, *58*, 570−592.
(7) Kawasaki, T. *J. Chromatogr., A* **1991**, *544*, 147−184.
(8) Kaneda, K.; Mori, K.; Hara, T.; Mizugaki, T.; Ebitani, K. *Catal. Surv. Asia* **2004**, *8*, 231−239.
(9) Elazarifi, N.; Chaoui, M. A.; Ouassouli, A. E.; Ezzamarty, A.; Travert, A.; Leglise, J.; de Ménorval, L.; Moreau, C. *Catal. Today* **2004**, *98*, 161−170.
(10) Mori, K.; Hara, T.; Mizugaki, T.; Ebitani, K.; Kaneda, K. *J. Am. Chem. Soc.* **2004**, *126*, 10657−666.
(11) Venugopal, A.; Scurrell, M. S. *Appl. Catal., A* **2003**, *245*, 137−147.
(12) Naganagowda, G. A.; Gururaja, T. L.; Levine, M. J. *J. Biomol. Struct. Dyn.* **1998**, *16*, 91−107.
(13) Schlesinger, D. H.; Hay, D. I. *J. Biol. Chem.* **1977**, *252*, 1689−1695.
(14) Raj, P. A.; Johnsson, M.; Levine, M. J.; Nancollas, G. H. *J. Biol. Chem.* **1992**, *267*, 5968−5976.
(15) Schwartz, S. S.; Hay. D. I.; Schlukebier, S. K. *Calcif. Tissue Int.* **1992**, *50*, 511−517.
(16) Ramasubbu, N.; Thomas, L. M.; Bhandary, K. K.; Levine, M. J. *Crit. Rev. Oral Biol. Med.* **1993**, *4*, 363−370.
(17) Gururaja, T. L.; Levine, M. J. *Pept. Res.* **1996**, *9*, 283−289.
(18) Long, J., R.; Dindot, J. L.; Zebroski, H.; Kiihne, S.; Clark, R. H.; Campbell, A., A.; Stayton., P. S.; Drobny, G. P. *Proc. Natl. Acad. Sci. U.S.A.* **1998**, *95*, 12083−12087.
(19) Shaw, W. J.; Long, J. R.; Dindot, J. L.; Campbell, A. A.; Stayton, P. S.; Drobny, G. P. *J. Am. Chem. Soc.* **2000**, *122*, 1709−1716.
(20) Shaw, W. J.; Long, J. R.; Stayton, P. S.; Drobny, G. P. *J. Am. Chem. Soc.* **2000**, *122*, 7118−7119.
(21) Long, J. R.; Shaw, W. J.; Stayton, P. S.; Drobny, G. P. *Biochemistry* **2001**, *40*, 15451−15455.
(22) Gibson, J. M.; Raghunathan, V.; Popham, J. M.; Stayton, P. S.; Drobny, G. P. *J. Am. Chem. Soc.* **2005**, *127*, 9350−9351.
(23) (a) Gullion, T.; Schaefer, J. *J. Magn. Reson.* **1989**, *81*, 196−200. (b) Gullion, T.; Schaefer, J. *Adv. Magn. Reson.* **1989**, *13*, 57−83.
(24) Goetz, J. M.; Schaefer, J. *J. Magn. Reson.* **1997**, *127*, 147−154.
(25) Goobes, G.; Raghunathan, V.; Louie, E. A.; Gibson, J. M.; Olsen, G. L.; Drobny, G. P. *Solid State Nucl. Magn. Reson.* **2006**, *29*, 242−250.
(26) Yesinowski, J. P. In *Calcium Phosphates in Biological and Industrial Systems*; Amjad, Z., Ed.; Kluwer: Boston, 1998.
(27) Pan, Y. *Solid. State Nucl. Magn. Reson.* **1995**, *100*, 15716−15725.
(28) Feike, M.; Demco, D. E.; Graf, R.; Gottwald, J.; Hafner, S.; Spiess, H. W. *J. Magn. Reson., Ser. A* **1996**, *122*, 214−221.
(29) Franke, D.; Banks, K.; Eckert, H. *J. Phys. Chem.* **1992**, *96*, 11048−11054.
(30) auf der Günne, J.; Eckert, H. *Chem.−Eur. J.* **1998**, *4*, 1762−1767.
(31) auf der Günne, J.; Eckert, H.; Leaustic, A.; Babonneau, F. *Phys. Chem. Chem. Phys.* **2003**, *5*, 1306−1313.
(32) auf der Günne, J. S.; Kaczmarek, S.; van Wullen, L.; Eckert, H.; Paschke, D.; Foecker, A. J.; Jeitschko, W. *J. Solid State Chem.* **1999**, *147*, 341−349.
(33) Bertmer, M.; Eckert, H. *Solid. State Nucl. Magn. Reson.* **1999**, *15*, 139−152
(34) auf der Günne, J. *J. Magn. Reson.* **2003**, *165*, 18−32.
(35) Montagne, L.; Revel, B.; Palavit, G. *Phosphorus Res. Bull.* **2001**, *12*, 203−210.
(36) Oyler, N. A.; Tycko, R. *J. Phys. Chem. B* **2002**, *83*, 1205−1216.
(37) Ishii, Y. *J. Chem. Phys.* **2001**, *114*, 8473−8483.
(38) Tseng, Y.; Mou, Y.; Mou, C.; Chan, J. C. C. *Solid State Nucl. Magn. Reson.* **2005**, *27*, 266−270
(39) Gullion, T.; Vega, S. *Chem. Phys. Lett.* **1992**, *194*, 423−428

(40) Gregory, D. M.; Mitchell, D. J.; Stringer, J. A.; Kiihne, S.; Shiels, J. C.; Callahan, J.; Mehta, M. A.; Drobny, G. P. *Chem. Phys. Lett.* **1995**, *246*, 654−663.

(41) Mehta, M. A.; Gregory, D. M.; Kiihne, S.; Mitchell, D. J.; Hatcher, M. E.; Shiels, J. C.; Drobny, G. P. *Solid State Nucl. Magn. Reson.* **1996**, *7*, 221−228.

(42) Gregory, D. M.; Mehta, M. A.; Shiels, J. C.; Drobny, G. P. *J. Chem. Phys.* **1997**, *107*, 28−42.

(43) Stringer, J. A.; Drobny, G. P. *Rev. Sci. Instrum.* **1998**, *69*, 3384−3391.

(44) Ishii, Y.; Ashida, J.; Terao, T. *Chem. Phys. Lett.* **1995**, *246*, 439−45

(45) Bak, M.; Rasmussen, J. T.; Nielsen, N. C. *J. Magn. Reson.* **2000**, *147*, 296−330.

(46) Veshtort, M.; Griffin, R. G. *ChemPhysChem* **2004**, 5, 834−850.

(47) Conroy, H. *J. Chem. Phys.* **1967**, *47*, 5307.

(48) Cheng, V., B.; Suzukawa, H., H.; Wolfsberg, M. *J. Chem. Phys.* **1973**, *59*, 3992

(49) Herzfeld, J.; Berger, A. E. *J. Chem. Phys.* **1980**, *73*, 6021−6030.

(50) Eichele, K.; Wasylishen, R. E. *HBA*, version. 1.4.4; Dalhousie University: Halifax, Canada, 2004.

(51) Duncan, T. M. *Chemical Shift Tensors*; Farragut Press: Madison, WI, 1997.

(52) Herzfeld, J.; Griffin, R. G.; Haeberkorn, R. A. *Biochemistry* **1978**, *17*, 2711−2718.

(53) Un, S.; Klein, M. P. *J. Am. Chem. Soc.* **1989**, *111*, 5119−5124.

(54) Kohler, S. J.; Ellet, J. D.; Klein, M. P. *J. Chem. Phys.* **1976**, *64*, 4451−4458.

(55) Khan, A. A.; Roux, J. P.; James, W. J. *Acta Crystallogr., Sect. B* **1978**, *28*, 2065−2069

(56) Elliott, J. C.; Mackie, P. E.; Young, R. A. *Science* **1973**, *180*, 1055−1057

(57) Hochrein, O.; Kniep, R.; Zahn, D. *Chem. Mater.* **2005**, *17*, 1978−1981.

(58) Goobes, G.; Vega, S. *J. Magn. Reson.* **2002**, *154*, 236−251.

(59) Taylor, J. R. *An Introduction to Error Analysis*; University Science Books: Mill Valley, CA, 1982.

(60) Nadassy, K.; Wodak, S. J.; Janin, J. *Biochemistry* **1999**, *38*, 1999−2017.

(61) Burget, U.; Zundel, G. *J. Mol. Struct.* **1986**, *145*, 93−109.